Solar Phys (2011) 273:493–509
DOI 10.1007/s11207-011-9872-9

The 17 January 2005 Complex Solar Radio Event Associated with Interacting Fast Coronal Mass Ejections

A. Hillaris · O. Malandraki · K.-L. Klein · P. Preka-Papadema · X. Moussas · C. Bouratzis · E. Mitsakou · P. Tsitsipis · A. Kontogeorgos

Received: 31 January 2011 / Accepted: 20 September 2011 / Published online: 8 November 2011

Abstract On 17 January 2005 two fast coronal mass ejections were recorded in close succession during two distinct episodes of a 3B/X3.8 flare. Both were accompanied by metre-

Energy Storage and Release through the Solar Activity Cycle – Models Meet Radio Observations
Guest Editors: Christophe Marqué and Alexander Nindos

A. Hillaris (✉) · P. Preka-Papadema · X. Moussas · C. Bouratzis · E. Mitsakou
Section of Astrophysics, Astronomy and Mechanics, Department of Physics, University of Athens, Zografos (Athens), 15783, Greece
e-mail: ahilaris@phys.uoa.gr

P. Preka-Papadema
e-mail: ppreka@phys.uoa.gr

X. Moussas
e-mail: xmoussas@phys.uoa.gr

C. Bouratzis
e-mail: kbouratz@phys.uoa.gr

E. Mitsakou
e-mail: emitsaku@phys.uoa.gr

O. Malandraki
Institute of Astronomy and Astrophysics, National Observatory of Athens, 11810 Athens, Greece
e-mail: omaland@astro.noa.gr

K.-L. Klein
Observatoire de Paris, LESIA-CNRS UMR 8109, Univ. Paris 6 & Paris 7, Observatoire de Meudon, 92195 Meudon, France
e-mail: ludwig.klein@obspm.fr

P. Tsitsipis · A. Kontogeorgos
Technological Educational Institute of Lamia, 35100 Lamia, Greece

P. Tsitsipis
e-mail: tsitsipis@teilam.gr

A. Kontogeorgos
e-mail: akontog@teilam.gr

to-kilometre type-III groups tracing energetic electrons that escape into the interplanetary space and by decametre-to-hectometre type-II bursts attributed to CME-driven shock waves. A peculiar type-III burst group was observed below 600 kHz 1.5 hours after the second type-III group. It occurred without any simultaneous activity at higher frequencies, around the time when the two CMEs were expected to interact. We associate this emission with the interaction of the CMEs at heliocentric distances of about 25 $R_{\odot}$. Near-relativistic electrons observed by the EPAM experiment onboard ACE near 1 AU revealed successive particle releases that can be associated with the two flare/CME events and the low-frequency type-III burst at the time of CME interaction. We compare the pros and cons of shock acceleration and acceleration in the course of magnetic reconnection for the escaping electron beams revealed by the type-III bursts and for the electrons measured *in situ*.

Keywords Radio bursts, meter-wavelengths and longer (m, dkm, hm, km) · Coronal mass ejections · Energetic particles, acceleration · Energetic particles, electrons · Energetic particles, propagation

1. Introduction

The acceleration of charged particles to high energies in the solar corona is related to flares, which reveal the dissipation of magnetically stored energy in complex magnetic-field structures of the low corona, and to coronal mass ejections (CMEs), which are large-scale, complex magnetic-field–plasma structures ejected from the Sun. CMEs can drive bow shocks, and their perturbation of the coronal magnetic field can also give rise to magnetic reconnection, where energy can be released in a similar way as during flares.

When several CMEs are launched along the same path, a faster CME may overtake a slower preceding one, and the two CMEs can merge into a single structure. For this phenomenon Gopalswamy *et al.* (2001) introduced the term *CME Cannibalism*. The CME–CME interaction was found to be associated with a characteristic low-frequency continuum radio emission. Gopalswamy *et al.* (2002) interpreted this type of activity as the radio signature of non-thermal electrons originating either during reconnection between the two CMEs or as the shock of the second, faster CME travels through the body of the first (see Schmidt and Cargill, 2004 for a numerical study of two interacting coronal mass ejections).

In this paper we use radio diagnostics to study electron acceleration during a complex solar event broadly consisting of two stages, each associated with a distinct episode of a flare and with a fast CME, which occurred in close temporal succession on 17 January 2005. The CMEs interacted at a few tens of $R_{\odot}$. Both the flare/CME events and the CME interaction were accompanied by radio emission, which is used here to study electron acceleration scenarios. Energetic electrons in the corona and interplanetary space are traced by their dm-to-km-wave radio emission, mostly excited at or near the electron plasma frequency. The emission provides a diagnostic of the type of the exciter and its path from the low corona (cm–dm wavelengths) to 1 AU (km wavelengths). Radio emissions from exciters moving through the corona appear in dynamic spectra as structures exhibiting a drift in the time–frequency domain. The drift rate depends on their speed and path, resulting in a variety of bursts. Type-III bursts trace the path of supra–thermal electrons guided by magnetic structures. They appear, on dynamic spectra, as short structures (lasting from a fraction of a second at dm-waves to a few tens of minutes at km-waves) with fast negative drift ($\frac{1}{f}\frac{\mathrm{d}f}{\mathrm{d}t} \approx 0.5\ \mathrm{s}^{-1}$; see for example Güdel and Benz, 1988). This corresponds to anti-sunward propagation of the electrons through regions of decreasing ambient density at

speeds $\approx c/3$ (*e.g.*, Suzuki and Dulk, 1985). Sunward travelling beams produce reverse drift bursts (RS bursts), and beams propagating in closed loops emit type-U or -J bursts comprising a succession of an initial drift towards lower frequencies and a more or less pronounced RS burst.

Type-II bursts are more slowly drifting bursts ($\frac{1}{f}\frac{\mathrm{d}f}{\mathrm{d}t} \approx 0.001 - 0.01\ \mathrm{s}^{-1}$; see, for example, Table A.1 in Caroubalos *et al.*, 2004) excited by electrons accelerated at travelling shocks and emitting in their upstream region. Finally broadband dm–m wave continuum emission that may last over several minutes or even hours (type-IV burst) is ascribed to electrons confined in closed coronal magnetic structures. The reader is referred to the reviews in McLean and Labrum (1985), Bastian, Benz, and Gary (1998), Nindos *et al.* (2008) and Pick and Vilmer (2008) for more detailed accounts of the radio emission by non-thermal electrons in the corona.

2. Observations and Data Analysis

The 17 January 2005 event consisted of a complex flare, two very fast coronal mass ejections (CMEs), and intense and complex soft X-ray (SXR) and radio emission. In all radiative signatures two successive stages can be distinguished. The CMEs were launched successively from neighbouring regions of the corona and interacted in interplanetary space. The sequence of the observed energetic phenomena is summarized in Table 1 and described, in detail, in the following subsections.

2.1. Optical Observations: Flares and CMEs

Figure 1 displays snapshots in the Hα line obtained from the Kanzelhöhe solar observatory (courtesy M. Temmer; see also Temmer *et al.* (2007), Figure 2, for details on the evolution of the Hα flare ribbons). The only major active region on the disk is NOAA 10720 in the north-western quadrant (N15° W25°). It displayed nearly uninterrupted activity since the early hours of 17 January 2005. The most conspicuous event was a 3B Hα flare reported by Kanzelhöhe 09:16 – 11:57 UT. This flare proceeded successively in two different parts of AR 10720, as shown in the two snapshots of the bottom panel. The first part of the event, referred to as "stage 1" (illustrative snapshot at 09:13 UT), is seen in the eastern part of the active region, close to the sunspots. It is associated with the temporary disappearance or eruption of the filament labelled 'F1' in the upper right panel. Two major flare ribbons are distinguished in the snapshot at 09:13 UT: a narrow band essentially in the east–west direction and a broader north–southward oriented region. The significant offset of the two ribbons with respect to the neutral line shows the eruption of a strongly sheared magnetic field. After about 09:35 UT the brightest emission is seen in the western part of the active region ("stage 2" ; see snapshot at 09:54 UT), together with the eruption of another filament 'F2' (or of a different part of the filament whose northern section erupted before). The brightening consisted of two essentially parallel flare ribbons, which were connected by post flare loops in later snapshots (not shown here). These two stages of the event were also found in the soft X-ray (SXR) and radio emissions, as will be discussed below.

Two CMEs were observed in close succession. A sequence of difference images from the *Large Angle and Spectrometric Coronagraph* (LASCO) aboard the SOHO spacecraft (Brueckner *et al.*, 1995) is displayed in Figure 2: the first CME (henceforth CME_1) is seen in the image at 09:30 UT in the north-western quadrant. While it travelled through the corona, the second, broader CME (CME_2) appeared underneath (image at 09:54 UT). The most

Table 1 Overview of the 17 January 2005 Event and associated activity.

Event	Time UT	Characteristics	Remarks
SXR Start	06:59		AR10720 (N15° W25°)
Type IV	08:40	3.0 – 630 MHz	AR10720
CME_1	09:00		lift-off
SXR Stage 1	09:05		
First cm burst start	09:05		RSTN 15400 MHz
Type III_1	09:07 – 09:28	0.2 – 630 MHz	AR10720
Type II_1	09:11	0.2 – 5 MHz	AR10720
Hα Start	09:13	3B	KANZ, AR10720
CME_1	09:30	2094 km s^{-1}	On C2
HXR Start	09:35:36		RHESSI Number 5011710
CME_2	09:38		lift-off
SXR Stage 2	09:42		End SXR Stage 1
Second cm burst start	09:43		RSTN 15400 MHz
Type III_2	09:43 – 09:59	0.2 – 630	AR10720
HXR peak	09:49:42	7865 counts s^{-1}	
Type II_2	09:48	0.2 – 8 MHz	AR10720
SXR peak	09:52	X3.8	End SXR Stage 2
CME_2	09:54	2547 km s^{-1}	On C2
First rise Electron flux	10:00	38 – 315 keV	ACE/EPAM
SXR End	10:07		AR720
HXR End	10:38:52	53 152 112 total counts	RHESSI
Second rise Electron flux	12:00	38 – 315 keV	ACE/EPAM
Type III_3	11:37	0.5 MHz	CME_1, CME_2 merge at 37 $R_\odot$ type II_2 overtakes type II_1
Hα End	11:57		KANZ
Type IV End	15:24	3.0 – 630 MHz	AR10720

conspicuous features of both CMEs are seen above the north-western limb, but both were labelled halo CMEs in the LASCO CME catalog[1] (Yashiro *et al.*, 2004). Speeds of, respectively, 2094 and 2547 km s^{-1} were derived from linear fits to the trajectories of their fronts published in the CME catalogue. Formally the CME fronts described by the fits intersected near 12:32 UT at a heliocentric distance of about 38 $R_\odot$. The statistical error of the speeds of the CME fronts and their lift-off times, derived from the above mentioned linear least-squares fit to the measured heliocentric distances, leads to an uncertainty of ± 3 h in the time

[1] http://cdaw.gsfc.nasa.gov/CME_list/.

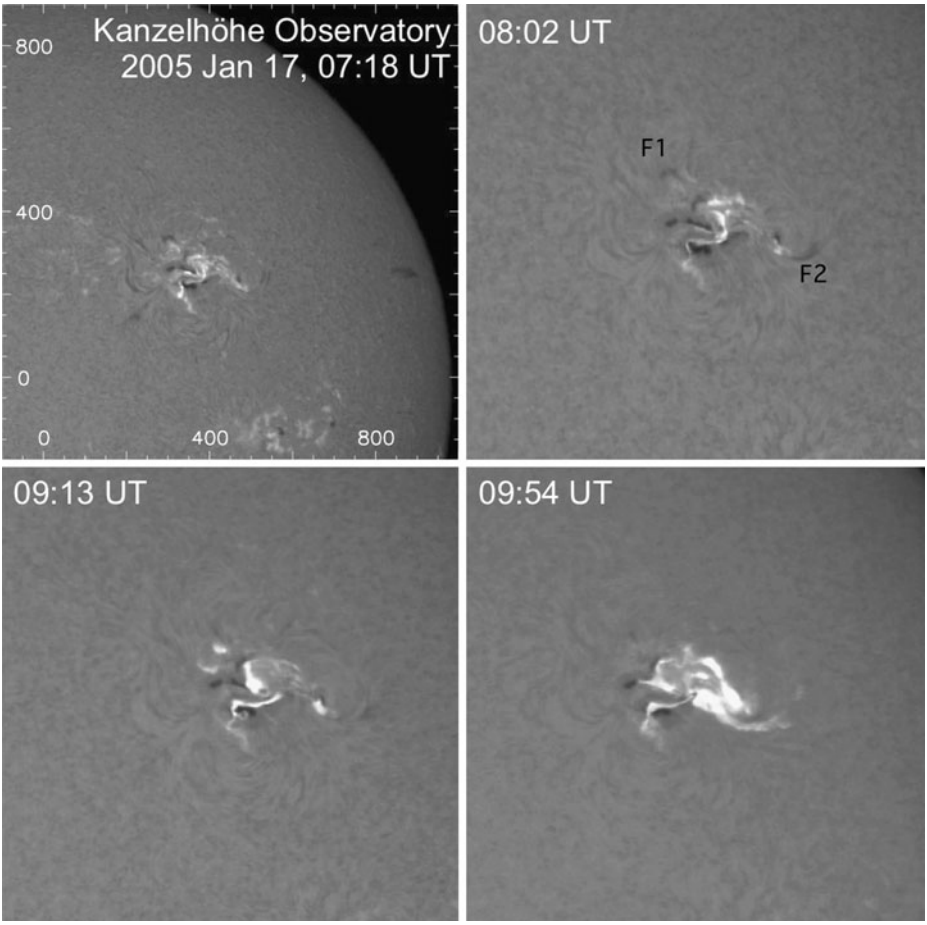

Figure 1 Snapshots of active region NOAA 10720 on 17 January 2005 in Hα line centre (top left) and in the wing, observed at Kanzelhöhe Observatory (courtesy M. Temmer). Solar north is at the top, west on the right. The two snapshots at the top show the active region before the flare under discussion, the two bottom images show two instants during the stages 1 and 2, respectively. These stages were associated with the disappearance of the filaments labelled 'F1' and 'F2'.

of intersection. This uncertainty stems from the fact that the two height–time trajectories are nearly parallel. We will show in Section 2.5 that CME interaction actually occurred well before the formal time of intersection. Of course a single instant of interaction between two complex CMEs is fictitious anyway.

2.2. Soft X-Ray and Radio Emission

An overview of the complex radio event is given in Figure 3. There we present the dynamic flux density spectrum of the radio bursts in the 650 MHz – 20 kHz range (heliocentric distance $\approx 1.1\ R_{\odot}$ to 1 AU) using combined recordings of the *Appareil de Routine pour le Traitement et l'Enregistrement Magnétique de l'Information Spectrale* (ARTEMIS-IV) solar radio-spectrograph (Caroubalos *et al.*, 2001; Kontogeorgos *et al.*, 2006) and the

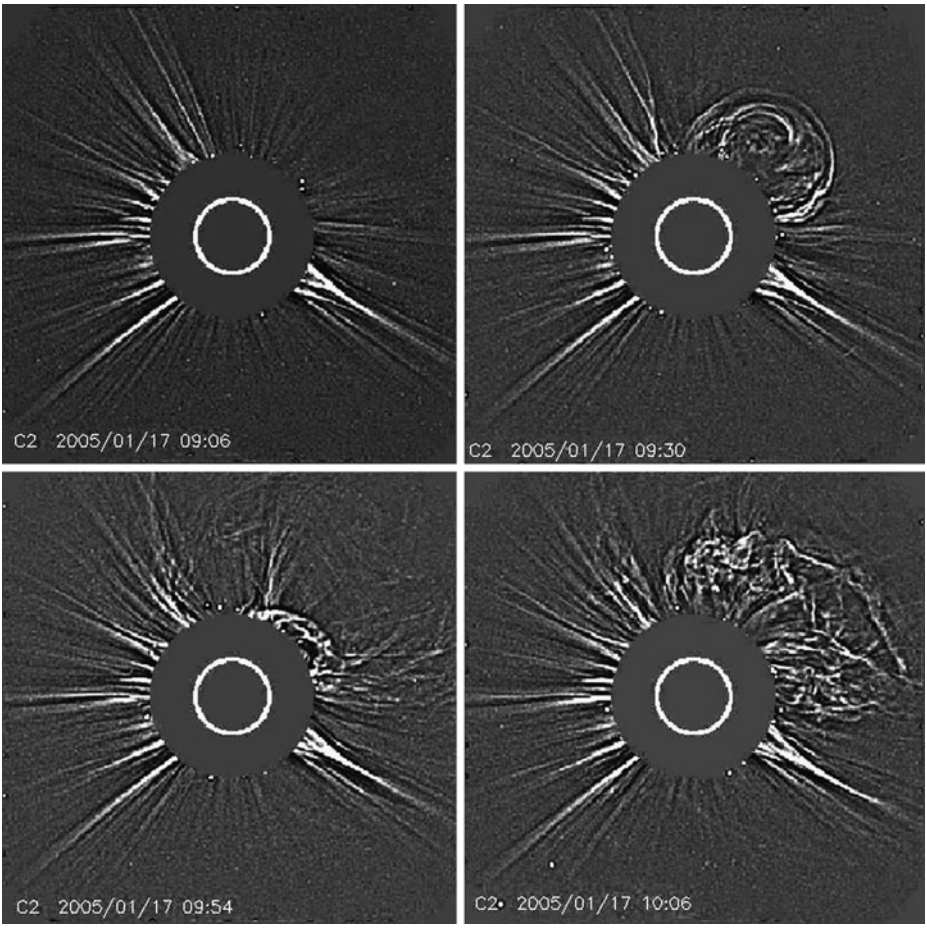

Figure 2 The two LASCO CMEs in close succession; the images have been subjected to high-pass filtering. Top: two frames of the 09:30:05 Halo CME with back-extrapolated lift-off at 09:00:47 UT and plane-of-the-sky speed 2094 km s^{-1}. Bottom: two frames of the 09:54:05 Halo CME with back-extrapolated lift-off at 09:38:25 UT and plane-of-the-sky speed 2547 km s^{-1}. Solar north is at the top, west on the right.

Wind/WAVES experiment (Bougeret *et al.*, 1995). Several other time histories are superposed on the dynamic spectrum:

- Dashed lines display the approximate frequency–time trajectories of the two CME fronts, using the density model of Vršnak, Magdalenić, and Zlobec (2004), which describes well the coronal density behaviour in the large range of distances from low corona to interplanetary space:

$$\frac{n}{10^8\ \mathrm{cm}^{-3}} = 15.45\left(\frac{R_\odot}{R}\right)^{16} + 3.165\left(\frac{R_\odot}{R}\right)^{6} + 1.0\left(\frac{R_\odot}{R}\right)^{4} + 0.0033\left(\frac{R_\odot}{R}\right)^{2}.$$

  The linear fits to the height–time trajectories of the CME fronts in the LASCO images were converted to frequency–time tracks of fundamental (black line) and harmonic (red line) plasma emission.

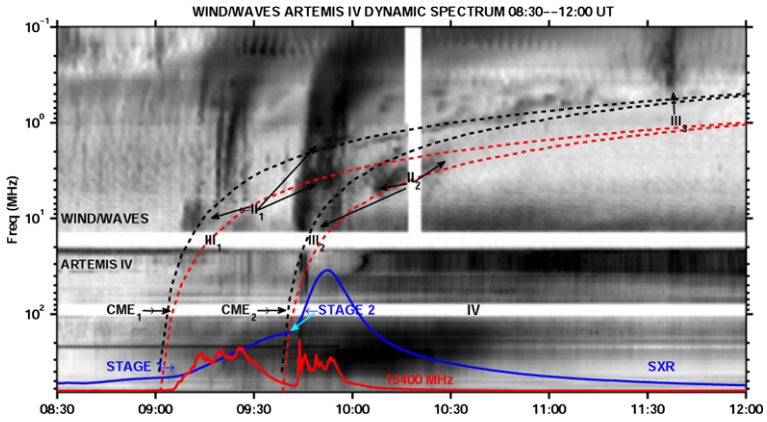

Figure 3 ARTEMIS-IV/*Wind*/WAVES dynamic spectrum (inverse grey scale). Overlays: The profiles of GOES SXR flux (dark blue) and RSTN flux density at 15400 MHz (red) and the frequency–time plots derived from the linear fits to the front trajectories of CME_1 and CME_2 and an empirical density model for fundamental (black dashed curve) and harmonic (red dashed curve) plasma emission. The type-IV continuum, the type-II (II_1 and II_2) and type-III GG bursts (III_1 and III_2), the stages 1 and 2 of the SXR flux rise, and the type-III burst (III_3) around the convergence of the fronts of CME_1 and CME_2 are annotated on the plot.

- The solid blue curve displays the SXR time history (0.1 – 0.8 nm), using GOES on line data (http://www.sel.noaa.gov/ftpmenu/indices), describing thermal emission from the flare-heated plasma.
- The red curve is the microwave time history at 15.4 GHz, produced by non-thermal electrons (energies > 100 keV) in magnetic fields of a few hundred G; these were obtained from the San Vito Solar Observatory of the Radio Solar Telescope Network (RSTN) (Guidice *et al.*, 1981).[2]

The two stages of the flare identified in the Hα observations in Figure 1 correspond to two distinct events of energy release seen in the SXR and microwave time profiles (Figure 3). The SXR time profile had an initial smooth increase between 06:59 UT and 09:05 UT. Subsequently the SXR flux rose slightly faster until 09:45 UT (stage 1), and even faster (stage 2) until the X3.8 peak at 09:52 UT. The gradual rise in stage 1 and the faster rise in stage 2 were each accompanied by strong microwave bursts. The second burst was also observed in hard X-rays by RHESSI[3] (Lin *et al.*, 2002).[4]

2.3. Radio Emission: Decametre-to-Kilometre Waves

The dominant features in the dynamic spectrum observed by *Wind*/WAVES at frequencies below 2 MHz are two groups of type-III bursts, labelled III_1 and III_2. They occurred in association with the SXR and microwave emissions of stages 1 and 2, respectively, and with the two different parts of the Hα flare. The two type-III groups occurred near the extrapolated

[2] http://www.ngdc.noaa.gov/nndc/struts/form?t=102827&s=6&d=8,40,9.

[3] http://hesperia.gsfc.nasa.gov/getfiles/rhessi_data_search.html.

[4] During stage 1 of the SXR flare RHESSI was in the Earth's shadow, so there is no HXR burst associated with the first microwave burst.

lift-off times of the two CMEs. Radio images taken by the *Nançay Radioheliograph* (NRH; Kerdraon and Delouis, 1997) show that the sources are located in the north-western quadrant near the flaring active region.[5] Hence both flare episodes were efficient accelerators of electrons that escaped to the interplanetary space along open magnetic field lines rooted at or near the flare site. The second type-III group (type III_2) was followed by a more slowly drifting narrow-band burst (type II, labelled II_2) produced by a coronal shock wave. Upon closer inspection the spectrum suggests that similar drifting features can also be associated with the first flare episode, although the association is less evident. We label these bursts II_1 in Figure 3. Since the two CMEs are extremely fast, they are expected to drive shock waves in the corona. The observed type-II emission can be compared with the dashed curves in Figure 3, which track fundamental (black) and harmonic (red) emission expected from the trajectory of the CME front and the coronal density model. It is clear that this density model is only indicative, especially in the perturbed corona through which travels the second CME (see discussion in Subsection 2.4). We therefore associate type-II_1 and -II_2 to the bow shocks of the two CMEs, although other interpretations, like shocks on the flanks or shocks from a driver related to the flare, are not excluded.

2.4. Radio Emission: Metre Waves

The dm–m wave emission consisted of a type-IV continuum, the metre wave counterparts of the dekametre–hectometre (DH) type-III groups and of the type-II bursts.

The type-IV continuum started near 08:40 UT during the initial smooth increase of the SXR flux before stage 1. It was first visible as a grey background in the dynamic spectrum, and became progressively more intense. It dominated the metre wave spectrum during and after type III_2, and gradually penetrated to lower frequencies, down to 5 MHz. Images in the EIT 195 Å channel (Delaboudinière *et al.*, 1995) and in the 164 – 432 MHz range taken by the NRH indicate that the thermal (soft X-rays) and non-thermal (radio) emissions all originated near NOAA AR 10720. In the time interval from the start of the type-IV burst to the start of stage 1 a wealth of fine structures was recorded (see Bouratzis *et al.*, 2009). From the high-resolution observations in the 200 – 500 MHz range (see Figures 5, 6 for example) it appears that most bursts are broadband pulsations. Other fine structures of type-IV emission such as spikes, fibre bursts and zebra pattern appear occasionally (see Kuijpers, 1980 for a description of the fine structure of type-IV emission.

During type III_1 the spectral character of the radio emission was clearly different at frequencies below and above the inferred frequency–time track of the CME_1 (see Figure 3). On the low-frequency side of the track strong type-III bursts were prominent after about 09:22 UT. They were preceded by a less regular emission, which Reiner *et al.* (2008) label "complex type-III bursts" because of its varying flux density across the spectrum.

The metre wave counterpart on the high-frequency side of the estimated CME track consisted of a succession of spectral fine structures on the time scale of seconds, with different spectral characteristics superposed on the type-IV continuum, followed after 09:11 UT by the high-frequency extension of the dekametre–hectometre (DH) type-III group III_1. A more detailed view of the difference spectrum is given in the top panel of Figure 4, whilst high-resolution images of the fine structures are in Figure 5. Among these fine structures were broadband pulsations, bursts with ordinary and reverse drift, and fibre bursts due to whistlers travelling upwards in the corona (see Figure 5, *e.g.*, 09:16:20 – 09:16:45 UT). The variety

[5] We have used 164 – 432 MHz contours overlaid on EIT 19.5 Å images.

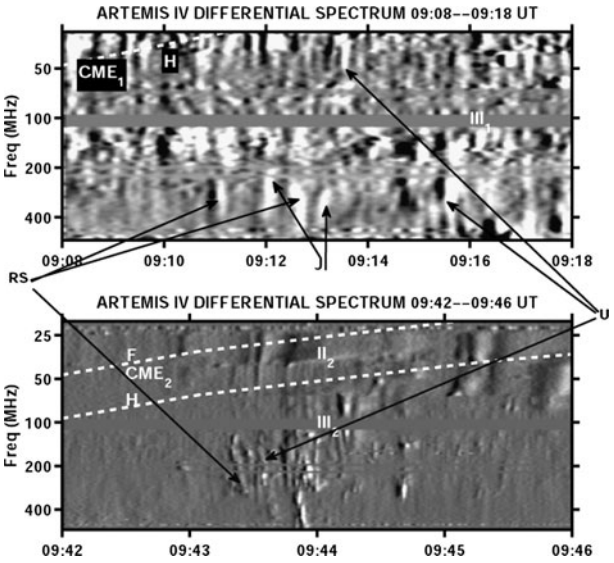

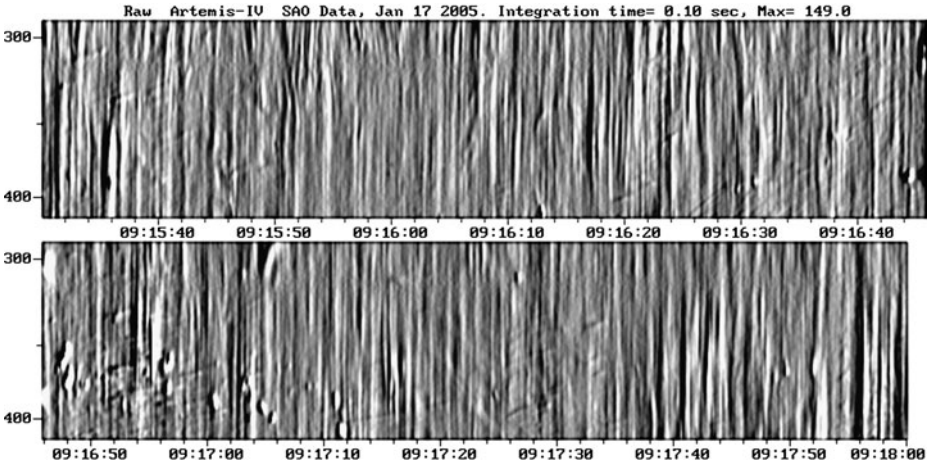

Figure 4 ARTEMIS IV differential spectra in the 20 – 550 MHz range. Top: type III_1 in the 09:08 – 09:18 UT interval. Some bursts of the type-III family (Reverse slope (RS), J-type, U-type) have been annotated. Bottom: type III_2 in the 09:42 – 09:46 UT interval. The frequency–time trajectories of CME_1 and CME_2 (white) are overlaid, assuming fundamental (F) and harmonic plasma emission.

Figure 5 ARTEMIS IV high-resolution (SAO) differential spectra in the 290 – 415 MHz range and the 09:15:30 – 09:18:00 UT interval.

of these bursts shows the acceleration and partial trapping of electron populations in the corona well behind the front of the CME. Indeed, few of the well-identified bursts above 100 MHz seem to continue into the 30 – 70 MHz range. It was only near the end of type III_1 ($\approx$ 08:18 UT) that metre wave type-III bursts appeared as systematic high-frequency extensions of the type-III bursts observed below 2 MHz.

Type III_2 started at 09:43 UT, together with the second microwave burst, near the back-extrapolated lift-off of CME_2 (09:38 UT) and the onset of stage 2 of the SXR burst. A close look at the dynamic spectrum (bottom panel of Figure 4) reveals negative overall drifts below 100 MHz, whilst burst groups with positive overall drift prevailed above 130 MHz. The high-resolution spectrogram in the 300 – 400 MHz range (Figure 6) shows a wealth of individual bursts with different drift rates and zebra pattern. These bursts show again, like in

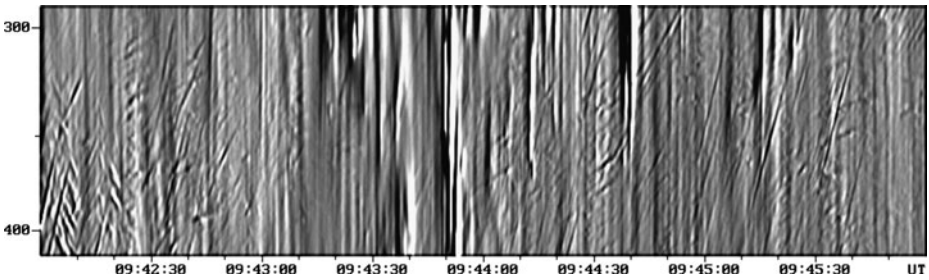

Figure 6 ARTEMIS IV high-resolution (SAO) differential spectra in the 290 – 415 MHz range and the 09:42 – 09:46 UT interval.

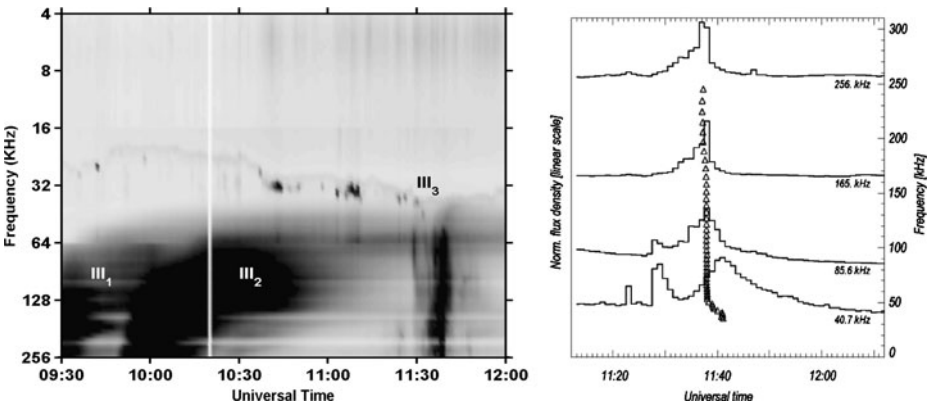

Figure 7 Kilometric radio bursts associated with the flares and with CME interaction. Left: WAVES/TNR dynamic spectrum (inverse grey scale) in the 4 – 256 kHz frequency range from 09:30 to 12:00 UT showing the burst groups type III_1, III_2 and III_3. Right: time histories during type III_3 (each normalized to its maximum) at selected frequencies. The open triangles show the time of maximum of the burst at each frequency in the range 35 – 256 kHz.

stage 1 of the event, that the high-frequency bursts are produced by an accelerator below the CME front, whilst low-frequency bursts show the start of the prominent DH type-III bursts.

2.5. Radio Emission and CME Interaction

Well after the decay of the SXR and microwave emission a third group of bursts (III_3 in Figure 3) is identified (near 11:30 UT), with unusually low starting frequency (0.6 MHz), pointing to an acceleration of the emitting electrons at unusually great height. A more detailed view of the low-frequency radio spectrum of this burst group and the preceding groups III_1 and III_2 is given by the dynamic spectrum as observed by the *Thermal Noise Receiver* (TNR) of *Wind*/WAVES in the left panel of Figure 7. The narrow-band short bursts near 32 kHz are Langmuir wave packets. Together with the fainter continuous band on which they are superposed they indicate how the electron plasma frequency evolves at the *Wind* spacecraft. At the time of III_3 it is about 35 kHz. Using a standard interplanetary density model, where the electron plasma frequency decreases as the inverse of the heliocentric distance R, the starting frequency of III_3 implies $R = 12\ R_\odot$ for fundamental plasma emission, and $R = 25\ R_\odot$ for the harmonic. From the LASCO observations and the uncertainties resulting from the straight-line fits to the CME front trajectories, the heliocentric distances of

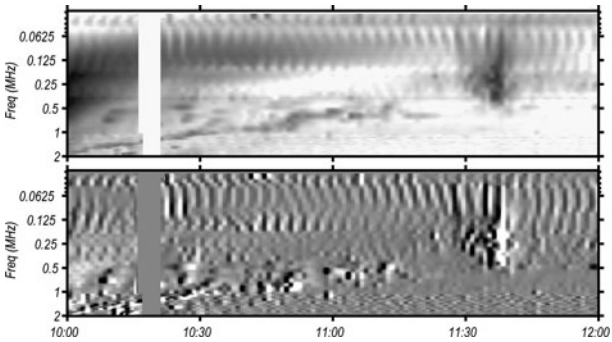

Figure 8 *Wind*/WAVES Spectra in the 2.0 – 0.03 MHz range with details of the merged type-II bursts (10:00 – 11:20 UT) and the low-frequency type III (III_3); about 11:30 – 11:40 UT). Top: intensity, bottom: differential.

the CME fronts at 11:30 UT are, respectively, $(26.9 \pm 4.8)\ R_\odot$ and $(24.5 \pm 5.5)\ R_\odot$. The burst group III_3 is hence consistent with harmonic emission from the vicinity of the CME fronts. This points to a close relationship of this episode of electron acceleration with the interaction of the two CMEs.

Comparison of the three groups of type-III bursts in the TNR spectrum of Figure 7 shows that type III_3 is much shorter than the previous type-III bursts. It has intrinsic structure that indicates a group of bursts. The low-frequency cutoff is near the plasma frequency at the spacecraft at that time. More details are seen in the selected time profiles in the right panel, plotted together with the peak times of the burst at each frequency in the 35 – 256 kHz range (open triangles). The time profiles show that the peak times are not distinguishable over a large part of the frequency spectrum with 1-min integrated data, but that the centre of gravity of the brightest feature shifts to later times at the lower frequencies. We determined the maximum of the burst at each of the TNR frequencies where it is well defined, using a parabolic interpolation between the observed maximum and its two neighbours. It is this interpolated time which is plotted by an open triangle. The peak time spectrum resembles a type-III burst especially at the lower frequencies. The peak time delay is merely 1 min between 250 and 50 kHz, but becomes clear at frequencies below 50 kHz. For comparison, the peak time delay between 50 and 250 kHz is 42 min during the previous burst III_2. The frequency drift rate is hence faster than 3 kHz s^{-1} during III_3, as compared to 0.08 kHz s^{-1} during III_2. Because of the morphological similarity in the dynamic spectrum, and despite the different drift rates, we assume in the following that the type-III_3 bursts are indeed produced by electron beams travelling in the anti-sunward direction from the acceleration region. Since the emission extends rapidly to the plasma frequency at the spacecraft, we conclude that the electron beams do not travel within the CMEs, but escape rapidly from the acceleration region in the vicinity of the CME fronts to 1 AU. This means that they must travel along pre-existing open solar wind field lines.

To the extent that drift rates reflect the speed of the exciter, the fast frequency drift of the type-III_3 bursts implies that the exciter speed is higher than during the preceding groups III_1 and III_2.

The total and differential radio spectrum observed by *Wind*/WAVES are shown in Figure 8. The spectrum shows a chain of narrow-band emissions with negative frequency drift, indicating the type-II bursts, followed by the high-frequency part of type III_3 between 11:28 and 11:40 UT. The spectrum in Figure 3 leaves it open if this is the continuation of the first type-II burst (II_1), presumably associated with CME_1, or whether it contains contributions from both CMEs. The starting frequency of the type-III bursts is similar to the type-II frequency when extrapolated to the time of the type-III bursts. This is consistent with the type-III electron beams radiating in the upstream region, like the shock-

accelerated electrons emitting the type-II burst. One may go one step further and consider this coincidence as a hint that the electron beams are accelerated at the shock, as argued in cases where type-III bursts clearly emanate from type-II lanes (see Bougeret *et al.*, 1998; Mann *et al.*, 2003). We will come back to this problem in the Discussion.

2.6. Solar Wind and Energetic Electrons Near 1 AU

The energetic particle data were obtained from the *Advanced Composition Explorer* (ACE) spacecraft. We use high-resolution intensities of magnetically deflected electrons (DE) in the energy range 38 – 315 keV measured by the B detector of the CA60 telescope of the EPAM experiment (*Electron, Proton and Alpha Monitor*; Gold *et al.*, 1998) on board ACE, and measurements of the angular distributions in the energy range 45 – 312 keV detected by the sunward looking telescope LEFS60. In Figure 9 (top) an overview of the 20-min averaged differential intensities of four channels is presented for the interval 15 – 20 January 2005. AR 10720 produced numerous solar events prior to as well as on 17 January 2005 (Malandraki *et al.*, 2007; Papaioannou *et al.*, 2010); in response to this solar activity, a sequence of energetic electron intensity enhancements was observed. The electron intensities are observed to reach their maximum values during this period following the solar events on 17 January 2005. Figure 9 (bottom) shows 1-min averaged deflected electron intensities (38 – 315 keV) for the time interval 04:00 – 20:00 UT on 17 January 2005. The intensities measured during the time interval 04:00 – 08:00 UT for each electron channel have been averaged to obtain a pre-event background (denoted by horizontal lines in Figure 9). We defined the onset time of the event at ACE for all energy channels as the time when the intensities get $> 2\sigma$ above the background and continue to rise from then on. Using this criterion, we found the first significant rise of the electron intensities to occur at 10:00 UT. No velocity dispersion was observed, probably because the high pre-event ambient intensities (see top panel Figure 9) mask the onset of the electron event (see Malandraki *et al.*, 2005, for a similar case). The spiky increase observed at about 10:40 UT is probably due to X-ray contamination. We found no evidence of a magnetic structure influencing the intensity profiles, which indicates the observed time intensity changes are not due to spatial structures crossing over the spacecraft, but are most likely dominated by temporal effects.

Twenty-minute averaged representative snapshots of pitch angle distributions (PADs) are shown as inserts in the bottom panel of Figure 9. Normalized differential electron intensity is plotted versus the cosine of the pitch angle. Statistically significant PADs are detected first at about 11:00 UT. The PAD snapshot denoted as a in Figure 9 indicates that immediately after the onset of the event unidirectional electron anisotropies are observed.

Based on the observations available we cannot distinguish whether the electrons were directed sunward or anti-sunward, since the magnetic field (not shown) was directed dominantly transverse to the radial direction during this period (see Figure 7 in Lario *et al.*, 2004 for a similar case). However, it is highly likely that the observed electrons are streaming away from the Sun in response to the intense solar activity during this period. Furthermore the type-III bursts clearly indicate that electrons stream away from the Sun (towards regions of lower density). We cannot be certain that the electron population measured at ACE/EPAM is the high-energy counterpart of the electron beams emitting the radio waves, yet the overall timing suggests this.

In the work by Papaioannou *et al.* (2010) a detailed analysis of the plasma and magnetic-field measurements at 1 AU by ACE during the period 16 – 26 January 2005 was carried out. This includes the period under study in the present paper. A forward shock was detected at 07:12 UT on 17 January 2005. We have denoted the arrival time of this shock by a vertical

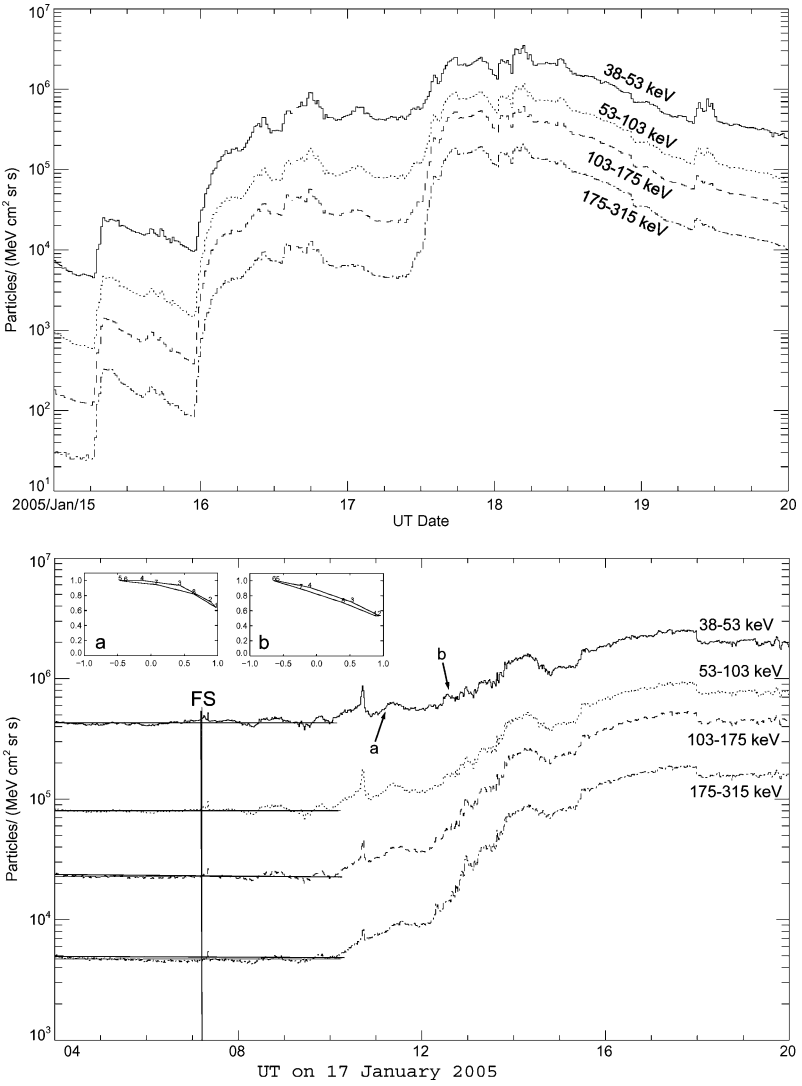

Figure 9 ACE/EPAM energetic electron enhancements in response to the 17 January 2005 solar activity. Top: 20-minute averaged differential intensities for the interval 15 – 20 January 2005. Labels of the abscissa are days. Bottom: 1-min averaged intensities (38 – 315 keV) for the interval 04:00 – 20:00 UT on 17 January 2005 of four magnetically deflected electron channels (38 – 315 keV) from the B detector head of the EPAM/CA60. Labels of the abscissa give the day (17 January) and the hour. The horizontal lines denote pre-event ambient intensity. The solid vertical line marks the arrival of an interplanetary forward shock (FS) at 07:12 UT at ACE. Inserts a and b present pitch angle distribution snapshots at the onset of the event at about 11:00 UT and at about 12:10 UT; normalized differential electron intensity is plotted *versus* the cosine of the pitch angle.

solid line in Figure 9 (bottom). The analysis has shown that after the passage of this shock an unusually extended region exhibiting sheath-like characteristics is observed for ≈ 1.5 day with highly variable magnetic-field magnitude and directions and typical to high proton temperatures (see Figure 3 of Papaioannou *et al.*, 2010 also Ruth Skoug, ACE/SWEPAM

PI team, private communication). This region is probably related to two CMEs ejected in close temporal sequence at the Sun on 15 January (see Figure 2 of Papaioannou *et al.*, 2010). Subsequently, at ≈ 23:00 UT on 18 January 2005 the arrival of an ICME at Earth is detected, ending at about 02:30 UT on 20 January.

The energetic electrons observed at 1 AU analyzed in this work were thus detected in the region with disturbed magnetic-field characteristics following the shock on 17 January 2005. For the purposes of this work, as an approximation, we calculated that the nominal Parker spiral for the measured solar wind speed of 620 km s^{-1} (ACE/SWEPAM) at the time of the rise of the electron intensity had a length of about 1.05 AU and was rooted near W 37° on the hypothetical solar wind source surface at 2.5 $R_{\odot}$. This longitude is not contradictory with an active region at W 25°, because non-radial coronal field lines can easily establish a connection (Klein *et al.*, 2008). Supposing that the early rise of the intensities was produced by the faster electrons in an energy channel moving along the interplanetary field line with 0 pitch angle, we estimate a travel time of about 15 min, which indicates the electrons were released from about 09:45 UT at the Sun. This corresponds to a photon arrival time at 09:53 UT. Given that our estimate of the electron rise gives only an upper limit, we consider that this electron release is related to type III_1 and type III_2 (Table 1), but cannot give a more detailed identification. The electron intensities are subsequently observed to exhibit a significant and more abrupt rise at all energies. Extrapolation of this second rise to the pre-event background intensities indicates a start at ≈ 12:00 UT. The electron PADs (inset b in Figure 9) indicate stronger unidirectional anisotropies are observed in association with this electron enhancement, which provides evidence for fresh injection of energetic electrons between the Sun and the spacecraft.

The outstanding radio emission near this time is the group of fast type-III bursts during the CME interaction, type III_3. If the electrons are accelerated at a heliocentric distance of about 25 $R_{\odot}$, the path travelled to the spacecraft along the nominal Parker spiral is 0.92 AU for the solar wind speed measured at the time of type III_3 (800 km s^{-1}). The inferred upper limit of the solar release time is 11:46 UT for 100 keV electrons. Photons released at that time at 25 $R_{\odot}$ (0.12 AU) will reach the Earth about 7 min later. Since the high background implies that our estimations of the electron rise times are upper limits, we consider that this timing is consistent with the type-III_3 burst group near 11:37 UT (Table 1). This process is hence accompanied by the acceleration of copious amounts of electrons that escape to the vicinity of the Earth.

3. Discussion and Conclusions

On 17 January 2005 two flare/CME events occurred in close temporal succession in the same active region. Both CMEs had very high projected speed, above 2000 km s^{-1}, but the second one was faster than the first and eventually overtook it. The CMEs were associated with two successive filament eruptions and SXR enhancements in the same active region. Since the filament eruptions occurred at neighbouring places in the parent active region, the CMEs probably resulted from the eruption of neighbouring parts of the same overall magnetic configuration. The soft X-ray characteristics of the two successive events were different: a slow monotonic rise to moderate flux during the first event, and a more impulsive rise to the X3.8 level (3.8×10^4 W m^{-2}) during the second. Both events had a conspicuous microwave burst, but the first one was stronger than the second, contrary to the soft X-rays. The second burst was also seen in hard X-rays by RHESSI, which was in the Earth's shadow during the first burst.

3.1. Evidence for Evolving Acceleration Regions in the Corona During the Flares

The decametre-to-hectometre wave spectra in the two stages looked similar, with bright groups of type-III bursts signalling the escape of electron beams at heliocentric distances beyond 2 $R_{\odot}$. But radio emission from lower heights shows distinctive differences that point to an evolving acceleration region, *i.e.* either an acceleration region which progresses through the corona or a number of acceleration sites activated in succession.

Shock acceleration was clearly at work during both stages of the flare, as shown by the type-II emission. The strong type-III bursts at the low-frequency side of the estimated spectral track of the CME front could also be ascribed to the acceleration at the type-II shock. The presence of type-III bursts with negative drift at higher frequencies and the fine structures of the type-IV continuum show, however, that at the time when the shock travelled through the high corona, other acceleration regions were active at lower altitude, as is usually the case during complex type-III bursts at decametre and longer waves (see Reiner *et al.*, 2008 and references therein). The type-III bursts (III_1) might then not start near the CME front, but at higher frequencies, and be interrupted by interactions of the electron beams with the turbulence near the front of CME_1. This is a frequently quoted interpretation of complex features in type-III bursts, both at kilometric (MacDowall, 1989) and decametric wavelengths (*e.g.* Reiner and Kaiser, 1999).

In the second type-III group (III_2) the overall frequency drift of the low resolution spectrum (Figure 4) was positive. The persistence of the metric type-IV burst, which suggested acceleration in the lower corona rather than at the shock during the first stage, is again a likely indication of an accelerator that was distinct from the CME shock, and acted in addition to the shock, at lower altitude. This is consistent with an interpretation of the electron acceleration in terms of reconnection in the corona behind the CME (Trottet, 1986; Cliver *et al.*, 1986; Kahler and Hundhausen, 1992). New evidence for this interpretation has recently been provided by Aurass, Landini, and Poletto (2009) using UV and white light coronographic diagnostics along with radio data.

3.2. CME Interaction and Related Radio Emission

Decametric–hectometric radio emission as a signature of CME interaction was discussed in some detail in two event studies (Gopalswamy *et al.*, 2001, 2002). In both events the radio emission had a limited bandwidth, and was referred to as a continuum. In the present case this emission is likely a set of type-III bursts and was therefore labelled type III_3. The starting frequency and the timing of these bursts are consistent with the idea that the electrons are accelerated whilst the faster following CME catches up with the slower preceding one.

The association of CME interaction with particle acceleration has been ascribed by Gopalswamy *et al.* (2001) to acceleration by the shock of the second CME as it traverses the previous one. Problems of this interpretation were discussed by Klein (2006).

Another important question is how the preceding CME could lead to strengthening of the shock of the following one. This problem is still more evident in the 17 January 2005 event, because here the two CMEs are already extremely fast and likely to drive strong shocks even in the ambient solar wind. Their relative speed, however, is rather slow, so that efficient acceleration by the shock of the second CME is not expected in the first CME. Another important feature is that the type-III_3 bursts extend to the plasma frequency at the spacecraft. The electrons hence cannot propagate in closed magnetic structures related to the CMEs. The accelerator must release the electron beams onto open solar wind-type field lines. An alternative scenario to acceleration at the CME shock is again magnetic reconnection. One

can surmise that these rapid CMEs were preceded by sheath regions with strong magnetic fields of interplanetary origin, draped around the CME front. These regions are favourable for magnetic reconnection (see the overview by Forsyth *et al.*, 2006 and references therein). The high pressure in the sheath of the second CME will be further enhanced when its progression is slowed down by the previous CME. This makes the configuration favourable to magnetic reconnection involving open solar wind field lines and strong magnetic fields, and allows one to understand qualitatively why accelerated electrons escape immediately towards the outer heliosphere.

In this scenario the type-III emission is expected to start close to the CME, in the upstream region. This can explain why the starting frequency is close to the frequency of the type-II burst, without implying that the electron beams were themselves accelerated at the shock.

3.3. Near-Relativistic Electrons at 1 AU

The flare/CME events under discussion were clearly related with enhanced fluxes of near-relativistic electrons at 1 AU. The peak intensity measured by ACE, of order 10^6 $(\mathrm{MeV\,cm^2\,sr\,s})^{-1}$ in the 38 – 53 keV range, makes the event comparable to the most intense ones of the sample studied by Haggerty and Roelof (2002), as seen in their Figure 3a. The CME speed is well above the speeds of the CMEs identified in that sample (Simnett, Roelof, and Haggerty, 2002).

Since the energetic electrons were observed at 1 AU within the region exhibiting sheath-like characteristics following the shock on 17 January 2005, it is difficult to estimate electron travel times and to relate the *in situ* measurements to solar processes. But the observations strongly suggest that successive intensity increases are first due to the coronal acceleration in the flare/CME event, and then to an episode during the interaction of the two CMEs. The escape of these electrons to ACE confirms the view discussed above that the electrons cannot have been accelerated in the body of the first CME, even if a shock driven by the second one passed through it. Neither can they originate from reconnection between closed magnetic field lines of the two CMEs. The electrons must rather be accelerated in regions from where they have ready access to solar wind magnetic field lines. This is consistent with a common acceleration of the mildly relativistic electrons and the electron beams at lower energies that produce the type-III_3 emission.

Acknowledgements This work was supported in part by the University of Athens Research Center (ELKE/EKPA). The authors appreciate discussions with and assistance of C. Caroubalos, C. Alissandrakis, and S. Hoang. They would also like to thank an anonymous referee for many useful comments on the original manuscript. Hα data were provided by the Kanzelhöhe Observatory, University of Graz, Austria by M. Temmer. The SOHO/LASCO data used here were produced by a consortium of the Naval Research Laboratory (USA), Max-Planck-Institut fuer Aeronomie (Germany), Laboratoire d'Astronomie (France), and the University of Birmingham (UK). The SoHO/LASCO CME catalog is generated and maintained at the CDAW Data Center by NASA and The Catholic University of America in cooperation with the Naval Research Laboratory. SOHO is a project of international cooperation between ESA and NASA. K.L.K. acknowledges the kind hospitality of the solar radio astronomy group at the University of Athens.

References

Aurass, H., Landini, F., Poletto, G.: 2009, *Astron. Astrophys.* **506**, 901.
Bastian, T.S., Benz, A.O., Gary, D.E.: 1998, *Annu. Rev. Astron. Astrophys.* **36**, 131.
Bougeret, J.-L., Kaiser, M.L., Kellogg, P.J., Manning, R., Goetz, K., Monson, S.J. *et al.*: 1995, *Space Sci. Rev.* **71**, 231.

Bougeret, J.-L., Zarka, P., Caroubalos, C., Karlický, M., Leblanc, Y., Maroulis, D. *et al.*: 1998, *Geophys. Res. Lett.* **25**, 2513.
Bouratzis, C., Preka-Papadema, P., Moussas, X., Alissandrakis, C., Hillaris, A.: 2009, *Adv. Space Res.* **43**, 605.
Brueckner, G.E., Howard, R.A., Koomen, M.J., Korendyke, C.M., Michels, D.J., Moses, J.D. *et al.*: 1995, *Solar Phys.* **162**, 357.
Caroubalos, C., Hillaris, A., Bouratzis, C., Alissandrakis, C.E., Preka-Papadema, P., Polygiannakis, J. *et al.*: 2004, *Astron. Astrophys.* **413**, 1125.
Caroubalos, C., Maroulis, D., Patavalis, N., Bougeret, J.L., Dumas, G., Perche, C. *et al.*: 2001, *Exp. Astron.* **11**, 23.
Cliver, E.W., Dennis, B.R., Kiplinger, A.L., Kane, S.R., Neidig, D.F., Sheeley, N.R., Koomen, M.J.: 1986, *Astrophys. J.* **305**, 920.
Delaboudinière, J.P., Artzner, G.E., Brunaud, J., Gabriel, A.H., Hochedez, J.F., Millier, F. *et al.*: 1995, *Solar Phys.* **162**, 291.
Forsyth, R.J., Bothmer, V., Cid, C., Crooker, N.U., Horbury, T.S., Kecskeméty, K., Klecker, B. *et al.*: 2006, *Space Sci. Rev.* **123**, 383.
Gold, R.E., Krimigis, S.M., Hawkins, S.E. III, Haggerty, D.K., Lohr, D.A., Fiore, E., Armstrong, T.P. *et al.*: 1998, *Space Sci. Rev.* **86**, 541.
Gopalswamy, N., Yashiro, S., Kaiser, M.L., Howard, R.A., Bougeret, J.L.: 2001, *Astrophys. J. Lett.* **548**, L91.
Gopalswamy, N., Yashiro, S., Kaiser, M.L., Howard, R.A., Bougeret, J.: 2002, *Geophys. Res. Lett.* **29**(8), 080000.
Güdel, M., Benz, A.O.: 1988, *Astron. Astrophys. Suppl. Ser.* **75**, 243.
Guidice, D.A., Cliver, E.W., Barron, W.R., Kahler, S.: 1981, *Bull. Am. Astron. Soc.* **13**, 553.
Haggerty, D.K., Roelof, E.C.: 2002, *Astrophys. J.* **579**, 841.
Kahler, S.W., Hundhausen, A.J.: 1992, *J. Geophys. Res.* **97**, 1619.
Kerdraon, A., Delouis, J.M.: 1997, In: Trottet, G. (ed.) *Coronal Phys. from Radio and Space Observations*, *Lecture Notes in Phys.* **483**, Springer, Berlin, 192.
Klein, K.-L.: 2006, In: Gopalswamy, N., Mewaldt, R., Torsti, J. (eds.) *Solar Eruptions and Energetic Particles*, *AGU Monogr.* **165**, Amer. Geophysical Union, Washington, 233.
Klein, K.-L., Krucker, S., Lointier, G., Kerdraon, A.: 2008, *Astron. Astrophys.* **486**, 589.
Kontogeorgos, A., Tsitsipis, P., Caroubalos, C., Moussas, X., Preka-Papadema, P., Hilaris, A. *et al.*: 2006, *Exp. Astron.* **21**, 41.
Kuijpers, J.: 1980, In: Kundu, M.R., Gergely, T.E. (eds.) *Radio Phys. of the Sun*, *IAU Symp.* **86**, 341.
Lario, D., Decker, R.B., Roelof, E.C., Reisenfeld, D.B., Sanderson, T.R.: 2004, *J. Geophys. Res.* **109**, 1107.
Lin, R.P., Dennis, B.R., Hurford, G.J., Smith, D.M., Zehnder, A., Harvey, P.R. *et al.*: 2002, *Solar Phys.* **210**, 3.
MacDowall, R.J.: 1989, *Geophys. Res. Lett.* **16**, 923.
Malandraki, O.E., Lario, D., Lanzerotti, L.J., Sarris, E.T., Geranios, A., Tsiropoula, G.: 2005, *J. Geophys. Res.* **110**, 9.
Malandraki, O.E., Marsden, R.G., Tranquille, C., Forsyth, R.J., Elliott, H.A., Lanzerotti, L.J., Geranios, A.: 2007, *J. Geophys. Res.* **112**, 6111.
Mann, G., Klassen, A., Aurass, H., Classen, H.T.: 2003, *Astron. Astrophys.* **400**, 329.
McLean, D.J., Labrum, N.R. (eds.): 1985, *Solar Radiophys.: Studies of Emission from the Sun at Metre Wavelengths*.
Nindos, A., Aurass, H., Klein, K.L., Trottet, G.: 2008, *Solar Phys.* **253**, 3.
Papaioannou, A., Malandraki, O., Belov, A., Skoug, R., Mavromichalaki, H., Eroshenko, E., Abunin, A., Lepri, S.: 2010, *Solar Phys.* **266**, 181.
Pick, M., Vilmer, N.: 2008, *Astron. Astrophys. Rev.* **16**, 1.
Reiner, M.J., Kaiser, M.L.: 1999, *Geophys. Res. Lett.* **26**, 397.
Reiner, M.J., Klein, K., Karlický, M., Jiřička, K., Klassen, A., Kaiser, M.L., Bougeret, J.: 2008, *Solar Phys.* **249**, 337.
Schmidt, J., Cargill, P.: 2004, *Ann. Geophys.* **22**, 2245.
Simnett, G.M., Roelof, E.C., Haggerty, D.K.: 2002, *Astrophys. J.* **579**, 854.
Suzuki, S., Dulk, G.A.: 1985, In: McLean, D., Labrum, N. (eds.) *Solar Radiophys.: Studies of Emission from the Sun at Metre Wavelengths*. Cambridge University Press, Cambridge, 289.
Temmer, M., Veronig, A.M., Vršnak, B., Miklenic, C.: 2007, *Astrophys. J.* **654**, 665.
Trottet, G.: 1986, *Solar Phys.* **104**, 145.
Vršnak, B., Magdalenić, J., Zlobec, P.: 2004, *Astron. Astrophys.* **413**, 753.
Yashiro, S., Gopalswamy, N., Michalek, G., St. Cyr, O.C., Plunkett, S.P., Rich, N.B., Howard, R.A.: 2004, *J. Geophys. Res.* **109**(18), 7105.